Research Square

Preprints are preliminary reports that have not undergone peer review.
They should not be considered conclusive, used to inform clinical practice,
or referenced by the media as validated information.

Strong Cu(I)–He interaction at open metal sites enables isotope-selective helium adsorption

Thomas Heine

thomas.heine@tu-dresden.de

TU Dresden https://orcid.org/0000-0003-2379-6251

Toshiki Wulf

University of Leipzig

Shubhajit Das

University of Leipzig

Elvira Dongmo

HZDR

Article

Keywords:

Posted Date: August 5th, 2025

DOI: https://doi.org/10.21203/rs.3.rs-7214188/v1

License: This work is licensed under a Creative Commons Attribution 4.0 International License.
Read Full License

Additional Declarations: There is **NO** Competing Interest.

Version of Record: A version of this preprint was published at Nature Communications on March 26th, 2026. See the published version at https://doi.org/10.1038/s41467-026-70901-6.

Strong Cu(I)–He interaction at open metal sites enables isotope-selective helium adsorption

Elvira Gouatieu Dongmo[+,1,2,3] *Toshiki Wulf*[2] *Shubhajit Das*[3] *Thomas Heine*[3,4,5]

1) Wilhelm-Ostwald-Institut für Physikalische und Theoretische Chemie, Universität Leipzig, Linnéstr. 2, 04103 Leipzig, Germany

2) Institute of Resource Ecology, Research Site Leipzig, Helmholtz-Zentrum Dresden-Rossendorf, Permoserstr. 15, 04318 Leipzig, Germany

3) Faculty of Chemistry and Food Chemistry, School of Science, TU Dresden, 01062 Dresden, Germany

4) Department of Chemistry and ibs for Nanomedicine, Yonsei University, Seodaemun-gu, Seoul 120-749, Republic of Korea

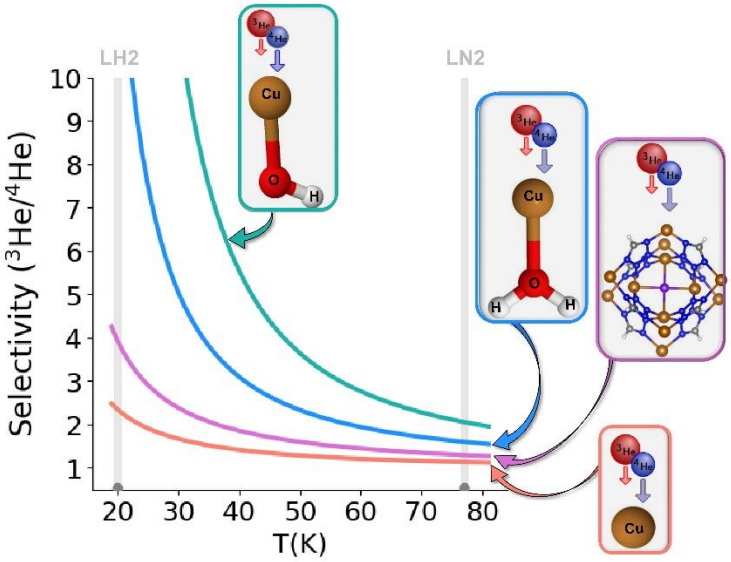
5) Center for Advanced Systems Understanding (CASUS) Untermarkt 20, 02826 Görlitz, Germany

Electronic mail: thomas.heine@tu-dresden.de

Abstract

The rare isotope helium-3 (^{3}He) is in very short supply on Earth and highly desired for various applications, including cryogenics, neutron detection and potentially as fuel for nuclear fusion reactors. The main terrestrial resources are tritium decay and the very small fraction in helium-4 dominated supplies obtained from natural gas. This calls for the development of efficient techniques for efficient separation of ^{3}He from isotope mixtures of He gas. In this study, we examine the circumstances that enable the selective adsorption of helium isotopes at open metal sites that commonly occur in metal–organic frameworks (MOFs) and zeolites. To this end, we first focus on small and computationally tractable model complexes of the transition metal Cu(I). We investigate the various aspects of bonding between the metal site and the adsorbed He using couple-cluster methods. In several of our model systems, we observe a substantial difference in adsorption zero-point energy between ^{3}He and ^{4}He, ranging from 0.2 kJ·mol^{-1} for

bare Cu^{+} to 0.7 kJ·mol^{-1} for the CuOH complex. For the latter, we predict a remarkable isotope selectivity of adsorption at the technologically relevant temperatures with separation factors of up to 47.2 at 20 K (liquid hydrogen, LH2) and 2.5 at 77 K (liquid nitrogen, LN2). This demonstrates the potential of adsorptive techniques for efficient helium isotope separation at highly attractive open metal sites with a suitable ligand environment. Encouraged by these findings, we expand our investigation to a series of realistic materials of varying complexity, ranging from crown ethers and porphyrins to zeolites and MOFs, as potential hosts for active Cu(I) sites. While all realistic systems exhibit more modest selectivity compared to the simpler model complexes, substantial selectivity approaching a separation factor of 4 is observed at LH2 temperature. Our results emphasize the crucial role of the ligand environment in enhancing selectivity. Among the studied systems, Cu(I) anchored at tetrahedral sites in zeolites and in m502_p3 MOF emerge as particularly promising candidates.



Introduction

The noble gas helium (He) is known for its chemical inertness, high volatility, and minimal polarizability, properties that usually prevent it from binding to any species. Surprisingly, as we demonstrate in that paper, helium exhibits a remarkably strong interaction with undercoordinated Cu(I) sites; an interaction strong enough to enable selective adsorption of ^{4}He over ^{3}He. This discovery is of fundamental interest to chemistry and opens the door for alternative ^{3}He production techniques.

Despite mechanical trapping (caging),[1] chemical interactions of helium seem to be impossible due to its low polarizability of 0.204×10^{-24} cm^3,[2] about 4 times smaller than that of H_2, its enormously high ionization potential of almost 25 eV, and its negligible electron affinity. Therefore, helium is considered to be an inert probe material, used for example to examine the porosity of materials using porosimetry or pycnometry.[3] Trapping helium typically involves tiny cages and gates, where spatial confinement hinders diffusion.[4] Studying the chemical affinity towards helium has been restricted to very few reports,[1] and to date, there are no reports to the best of our knowledge on exploiting chemical affinity to adsorb helium or even to separate its two stable isotopes, which include the most precious isotope on the planet, helium-3 (^{3}He).

^{3}He is a stable isotope with a natural abundance of 1.37 ppm as fraction of the total terrestrial helium occurrence, which is vastly dominated by helium-4, ^{4}He.[5–7] Its remarkable properties, in particular its fermionic character, make it a valuable material with significant applications in medicine for cooling MRI scanners, it provides shielding and leak-detection functionality in welding and electronics manufacturing and enables fundamental studies in cryogenics research.[8–10] Another potential use of ^{3}He is as fuel source in deuterium–helium-3 fusion reactors. As these reactors release high-energy protons (compared to neutrons in deuterium-tritium reactors), they can be operated more easily, making this technology an excellent candidate for clean energy generation [7,11]. The increasing global demand for ^{3}He,[5,12,13] combined with a lack of sources of production which still mainly rely on tritium decay,[14] call for alternative sources. Separation and purification of ^{3}He from natural helium supplies are currently being developed, but still require purification at about 2K.[15]

In this work, we demonstrate surprisingly strong interaction of He with Cu(I) sites, with adsorption enthalpies of up to ~12 kJ mol^{-1}. The interaction is predominantly governed by electron density sharing as revealed by a topological analysis of the electron density. Even though the adsorption enthalpy is significantly smaller than that of dihydrogen, it is sufficiently large to cause differences in zero-point energies (ZPEs) between the isotopes ^{3}He and ^{4}He. The ZPE difference enables chemical affinity quantum sieving (CAQS) as possible isotope separation technique at significantly higher temperature compared to the state of the art.[15] CAQS has been suggested for dihydrogen isotopologues in various metal-organic frameworks (MOFs)[16–20] and zeolites[21–23]. Among those, materials containing open Cu(I) centers have been found particularly promising due to differences

in adsorption enthalpies between H_2 and D_2 reaching 2.3−3 kJ mol^{-1} due to nuclear quantum effects (NQEs).[20,24,25]

We first studied small model complexes for which it was feasible to apply high-level theory both for the electronic interactions and for the NQEs, and thus predict the adsorption enthalpies and related isotope separation coefficients with high precision. We then derive a computational protocol that allows accurate predictions also for larger molecules (crown ethers and a metalloporphyrin) and clusters, the latter ones representing typical Cu(I) adsorption sites in MOFs and in zeolites. The MOF models have been obtained by a multistep filtering strategy: by observing the Cu(I) complexes are adsorbing strongest if coordinated to two, three or four ligands, we selected nine MOF systems created suitable model clusters to study their interaction with He. Among those, Cu(I)/UiO-66 and m502_p3 are most active, with adsorption enthalpies of 0.3 kJ mol^{-1}, and with a separation factor approaching 4 at LH2 temperature (20K).

Results and discussion

Model Cu(I) complexes

We have selected four Cu(I) complexes for initial conceptual and benchmark studies: two charged clusters Cu^+He and $Cu^+(H_2O)He$, which would be amenable to assessment in ion trap experiments as demonstrated for dihydrogen isotopes earlier,[26,27] and two uncharged ones, $Cu^+(OH^-)He$, and $Cu^+(H_2O)(OH^-)He$ (Fig. 1A). All structures have been fully optimized at the CCSD(T)/aug-cc-pVTZ level of theory. In all four model complexes we observe a strong Cu-He interaction. This is reflected in Born-Oppenheimer (BO) Cu–He bond distances ranging from 1.72 to 2.00 Å and BO adsorption energies (BSSE corrected) of –7.6 to –17.1 kJ mol^{-1}. The strongest interaction is found for the neutral $Cu^+(OH^-)$ cluster, which shows more than twice the adsorption energy compared to the bare Cu^+ ion (Fig. 1A, Tab. 1).

The unexpectedly strong Cu–He bonds are caused by two factors: as revealed by a quantum theory of atoms in molecules (QTAIM) analysis (PBE0-D3(BJ)/TZ2P, see Methods and Tab. S1), the bond critical points are located halfway between Cu and He. Electron density and Laplacian of electron density values for the $Cu^+(OH^-)He$ system being more than twice and five times as large as for the hydrogen bond in a water dimer. In the nonpolar Ar dimer, these values are significantly higher by a factor of 20 or more (Fig. 1A, see also Fig. S2). This indicates an usually strong polarization-driven interaction; as well as a slight covalent bonding nature[28]. Moreover, charge

transfer of about 0.1 electrons from the He to Cu centers (Hirshfeld charges, see Tab. 1) cause electrostatic attraction. We note, however, that the Hirshfeld charge transfer is very similar in all complexes and likely is an artifact of the charge accumulation between Cu and He. Indeed, the most strongly bound complexes $Cu^+(OH^-)He$ and $Cu^+(H_2O)(OH^-)$ show the largest density and Laplacian values at the bond critical points.

Vibrational frequencies have first been assessed analytically using the harmonic approximation (Tab. S2a and Tab. S3a). The significant degree of freedom for He adsorption is the Cu–He bond. Freezing all remaining degrees of freedom, we calculated the one-dimensional potential energy surface (PES) of the Cu–He coordinate from ~1.4 Å to bond dissociation (Fig. 1B). The strongly anharmonic character of the PES suggests that NQEs require a treatment beyond the harmonic approximation. As standard approaches such as VPT2 are computationally unfeasible at the target computational level for some of the systems, we developed an alternative approach: First, we freeze all degrees of freedom except for the He atom. Then, we calculate the PES of the Cu-He stretch mode while freezing all other degrees of freedom. The PES is fitted to a Morse potential augmented with a charge-induced dipole term (see Methods and Supplementary Note 1 for curve fitting details). We then solve the Schrödinger equation for the Cu-He stretch mode numerically using the finite difference method (FDM) and treat the two degrees of freedom of He normal to the Cu-He bond using the harmonic approximation. The latter is justified as Fig. S3 shows the PES of the vibrations normal to the Cu-He stretch mode and the extension of the vibrational state, which is well within the boundaries of the potential well. The results obtained with this protocol have been validated against VPT2 calculations (all at the MP2/def2-TZVP level, see Tab. S2a and Tab S2b). We call this approach "*numerical"* in the remainder.

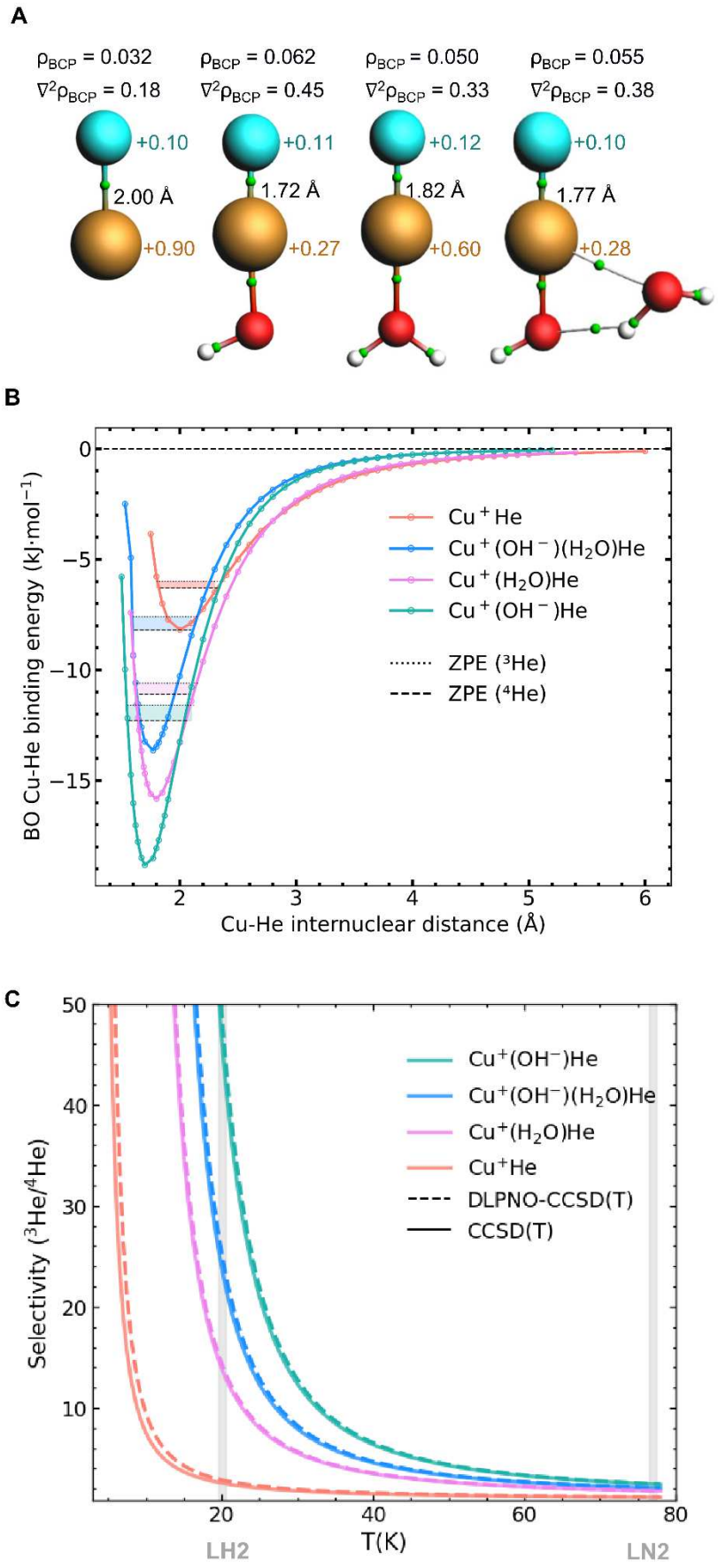

A
ρBCP = 0.032
∇²ρBCP = 0.18
+0.10
2.00 Å
+0.90
ρBCP = 0.062
∇²ρBCP = 0.45
+0.11
1.72 Å
+0.27
ρBCP = 0.050
∇²ρBCP = 0.33
+0.12
1.82 Å
+0.60
ρBCP = 0.055
∇²ρBCP = 0.38
+0.10
1.77 Å
+0.28
B
BO Cu-He binding energy (kJ·mol⁻¹)
0
−5
−10
−15
2
3
4
5
6
Cu-He internuclear distance (Å)
Cu⁺He
Cu⁺(OH⁻)(H₂O)He
Cu⁺(H₂O)He
Cu⁺(OH⁻)He
ZPE (³He)
ZPE (⁴He)
C
Selectivity (³He/⁴He)
50
40
30
20
10
20
40
60
80
T(K)
LH2
LN2
Cu⁺(OH⁻)He
Cu⁺(OH⁻)(H₂O)He
Cu⁺(H₂O)He
Cu⁺He
DLPNO-CCSD(T)
CCSD(T)

***Fig. 1**: **A)** Structures of the Cu^+He, $Cu^+(OH^-)He$, $Cu^+(H_2O)He$ and $Cu^+(H_2O)(OH^-)He$ complexes and results of the QTAIM analysis. Cu-He bond lengths (CCSD(T)/aug-cc-pVTZ level) are shown next to the bond paths and critical points as obtained by the QTAIM analysis, while Hirshfeld charges are shown for Cu (in brown) and He (in light blue) (PBE0-D3(BJ)/TZ2P level on CCSD(T)/aug-cc-pVTZ geometries). Colour scheme: Cu−brown, O−red, He−light blue, H−white. Bond critical points are shown as small green spheres. Values of the electron density ρ_{BCP} and its Laplacian $\nabla^2\rho_{BCP}$ are reported in atomic units (a.u.). **B)** Plot of the potential energy along the Cu–He stretch coordinate. All values are at the BSSE-corrected CCSD(T)/aug-cc-pVTZ level. ZPE-corrected adsorption energies (numerical method) are given for ^{3}He (dotted lines) and ^{4}He (dashed lines). **C)** Predicted separation factors for adsorptive He isotopes at low temperatures. All values are based on the CCSD(T)/aug-cc-pVTZ level (solid line) and DLPNO-CCSD(T)/cc-pVTZ(cu-He: aug-cc-pVTZ) (dashed line).*

To assess realistic materials models, the CCSD(T)/aug-cc-pVTZ level of theory is prohibitively expensive. We replace it with the computationally substantially more efficient DLPNO-CCSD(T) method[29,30], and use for all but the bond-related Cu and He atoms the smaller cc-pVTZ basis set. The results are in close agreement with the parent method, with Cu-He bonds differing by 0.02 Å or less, and adsorption energies by 1.6 kJ mol^{-1} or less (Tab. 1). Thus, the demonstrated reliability of DLPNO-CCSD(T) approach combined with numerical approach to calculate the ZPE offers a computationally efficient yet reference-grade protocol for larger cluster models with undercoordinated Cu(I) sites.

NQEs of all complexes have been calculated for the two stable isotopes of helium, ^{3}He and ^{4}He (Tab. 1). Quantum effects reduce the adsorption energies by 1.35 kJ mol^{-1} for Cu^+-^{4}He and 4.80 kJ mol^{-1} for $Cu^+(OH^-)$-^{4}He, and thereby slightly increase Cu-He distances (values for ^{4}He, all data Tab. 1). The ZPE increases, as expected, with the adsorption energy, but is also affected by the long-range asymptotics of the PES which shows a steeper decline for the charge-neutral complexes. This is reflected in the ZPE difference (ΔZPE) between the ^{3}He and ^{4}He isotopes, which strongly increases from 0.5 kJ mol^{-1} for $Cu^+(H_2O)$He for to 0.7 kJ mol^{-1} $Cu^+(OH^-)$He. The pronounced ΔZPE result in ^{3}He/^{4}He separation factors reaching 47.2 at liquid hydrogen (LH2) and even 2.5 at liquid

nitrogen (LN2) temperatures for $Cu^+(OH^-)He$ (Fig. 1C and Tab. S4). We note that the adsorption enthalpy is strong enough that the nearly all Cu(I) sites are occupied at these temperatures.

***Tab. 1**: Adsorption energies E_{ads}, and Cu-He bond lengths (d_{CuHe}) at the BSSE-corrected CCSD(T)/aug-cc-pVTZ and at the DLPNO-CCSD(T)/ cc-pVTZ(aug-cc-pVTZ for Cu and He) levels of theory (values given in the square brackets). Nuclear quantum effects are accounted for using the numerical approach (see text). For comparison, ZPE corrections using the harmonic approximation are given for the CCSD(T) calculations. Hirshfeld charges for Cu in the systems with adsorbed helium q_{CuHe} and for the adsorbed He atom q_{He}, electron density ρ_{BCP} at the BCP between Cu^+ and He .The ZPE difference is also benchmark for calculating Cu^+-He adsorption energies. All distances are expressed in Å and energy values in kJ·mol⁻¹.*

Systems	E_{ads}^{BO}	d_{CuHe}		E_{ads}^{0}		q_{CuHe} (e)	q_{He} (e)	ρ_{BCP} $(e \cdot r_{\mathrm{Bohr}})$	ΔZPE	
		^{3}He	^{4}He	^{3}He	^{4}He				analytical	numerical
Cu^+He	−7.6 [−8.7]	2.08 [2.07]	2.07 [2.06]	−6.0 [−7.2]	−6.3 [−7.3]	+0.900 [+0.897]	+0.101 [+0.103]	0.032 [0.034]	0.20 [--]	0.18 [0.19]
$Cu^+(OH^-)He$	−17.1 [−20.5]	1.77 [1.76]	1.76 [1.75]	−11.8 [−15.0]	−12.4 [−15.7]	+0.265 [+0.264]	+0.106 [+0.108]	0.062 [0.066]	0.71 [--]	0.66 [0.67]
$Cu^+(H_2O)He$	−14.4 [−16.5]	1.86 [1.85]	1.85 [1.84]	−10.6 [−12.7]	−11.1 [−13.2]	+0.599 [+0.597]	+0.120 [+0.122]	0.050 [0.052]	0.49 [--]	0.45 [0.47]
$Cu^+(H_2O)(OH^-)He$	−12.1 [−15.3]	1.82 [1.80]	1.81 [1.79]	−7.6 [−11.0]	−8.2 [−11.5]	+0.284 [+0.278]	+0.100 [+0.104]	0.055 [0.059]	0.59 [--]	0.55 [0.56]

Materials Models

Motivated by the strong Cu(I)–He interactions in the small gas phase model complexes we proceed to investigate the Cu(I)–He interaction in various cluster models of molecules and materials, *i.e.* crown ethers, porphyrins, zeolites, and metal-organic frameworks (MOFs). For all forthcoming calculations, we are using the established protocol: DLPNO-CCSD(T)/cc-pVTZ (aug-cc-pVTZ for Cu, He) level of theory, with the numerical method to account for NQEs.

The small, computationally feasible undercoordinated Cu(I) complexes of crown ethers, 6-crown-2 (6c2) and 9-crown-3 (9c3) (Fig. 2a), have been studied earlier for their hydrogen isotopologue adsorption.[31] In both cases, helium binds strongly to Cu(I). The Cu–He bond lengths are 1.81 Å and 1.89 Å for the (6c2)Cu^+ and (9c3)Cu^+ complexes, respectively, which is similar as for the small model Cu(I)-complexes discussed above. The BO adsorption energies are –12.4 and –8.4 kJ mol^{-1} (Tab. S9) and weaken to –9.6 (–9.2) and –6.1 (–5.9) for ^{4}He (^{3}He) when the ZPE is taken into account (Tab. 3). QTAIM analysis and charge redistribution (Tab. S6) with slightly weaker charge redistribution and density accumulation in the Cu-He bond are consistent with these values. Consequently, the differences in ZPE, ΔZPE, are 0.41 and 0.31 kJ mol^{-1} for the two clusters, resulting in remarkable ^{3}He/^{4}He separation factors of 9.7 (1.6) and 3.3 (1.2) at LH2 (LN2) temperature. The calculations suggest that both doubly and triply coordinated Cu(I) sites attract He strongly, with preference for the doubly coordinated site.

A tetracoordinated, planar Cu(I) can be realized, for example, in a metalloporphyrin (Fig. 2c). Metalloporphyrins have been used as linkers in various MOFs, in particular in surface-mounted MOFs where indium oxide rods are cross-linked with tetracoordinated metalloporphyrin linkers, so that the metal sites face a sufficiently large pore volume.[32] However, Cu(I)porphyrin shows very little attraction towards He (Tab. 3), with a Cu-He distance greater than 3.0 Å. We account this result to the planarity of Cu(I), and further will not consider tetracoordinated Cu(I) configurations.

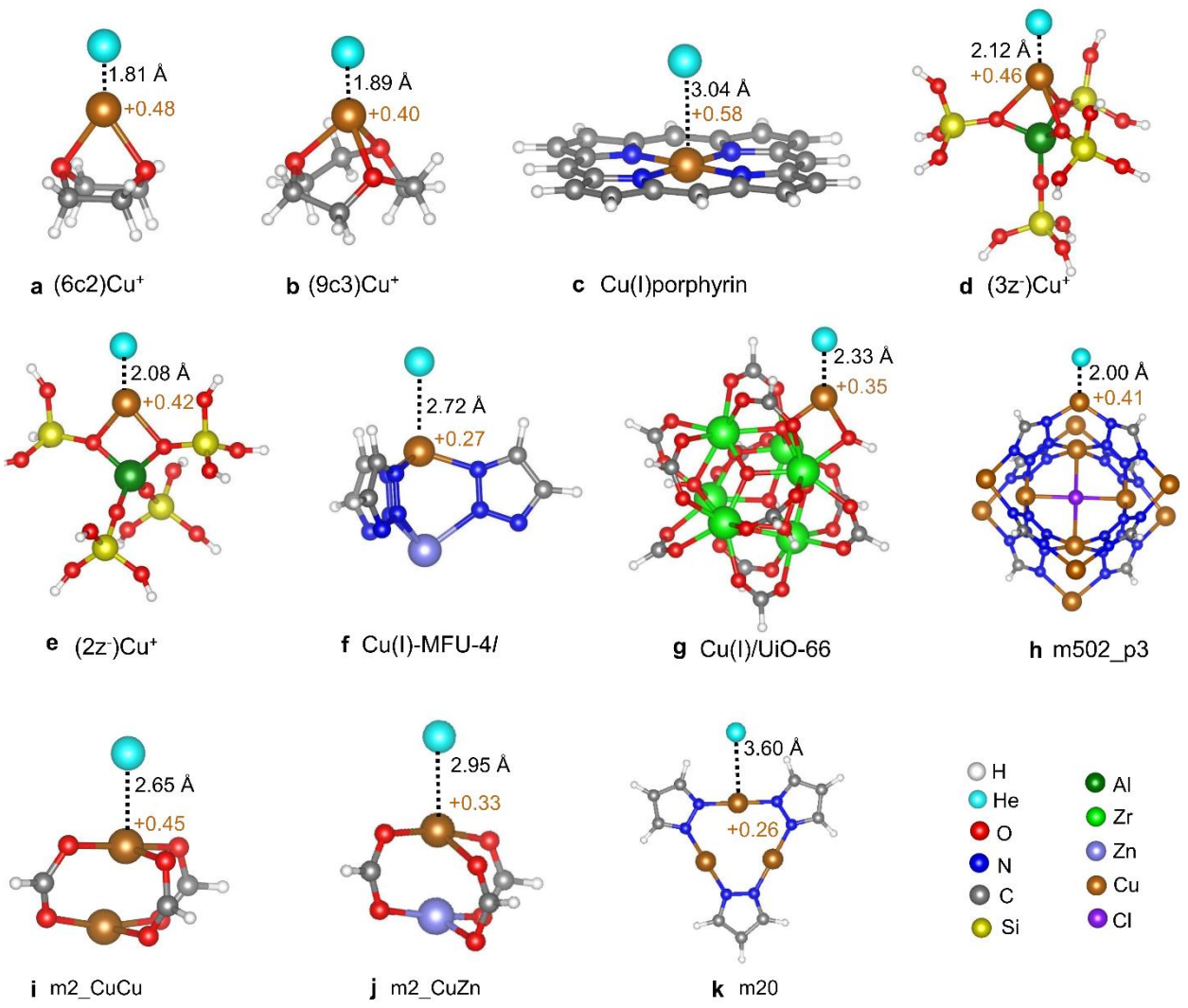


Fig. 2*: Atomistic models with adsorbed He atom at Cu(I) sites, indicating Cu–He bond lengths (black) and copper partial charges (brown). Crown-ether models:* ***a****, 6-crown-2 (6c2),* ***b****, 9-crown-3 (9c3).* ***c****, Cu(I)porphyrin. 5T zeolite cluster models with Cu^+coordinated to:* ***d****, three oxygen atoms [$(3z^-)Cu^+$] and* ***e****, two oxygen atoms [$(2z^-)Cu^+$]. Small structural models used to represent the SBUs of:* ***f****, Cu(I)-MFU-4l;* ***g****, Cu(I)/UiO-66;* ***h****, m502_p3;* ***i****, m2_CuCu;* ***j,*** *m2_CuZn with Zn substitution and* ***k****, m20.*

Based on an earlier work[31] we consider two zeolite model clusters with five tetrahedral sites (5T) that host undercoordinated Cu(I) centers (Fig. 2d-e) . In the first one, Cu(I) is coordinated by two

oxygen atoms ($2z^-$). This model is representative for common zeolites such as CHA, LTA und RHO, whereas the tri-coordinated model ($3z^-$) is representative for, e.g., zeolite LTA. Both zeolite models show weaker attraction to helium compared to the crown ethers. The Cu–He bond length exceeds 2 Å (2.12 for the $2z^-$ and 2.08 for the $3z^-$ model), resulting in BO adsorption energies of −3.3 and −4.7 kJ mol^{-1} for the two complexes (Tab. S9), respectively. NQEs further reduce the adsorption energy to −2.3 (−2.1) for the $2z^-$ model and −3.5 (−3.4) for the $3z^-$ model for ^{4}He (^{3}He). This results in ΔZPE of 0.14 and 0.16 kJ·mol^{-1}, which results in ^{3}He/^{4}He separation factors of 1.9 and 2.3 for LH2 temperature.

Tab. 3*: Geometrical Parameters of the material models studied in this work (all with adsorbed He). Bond lengths and energies at the DLPNO-CCSD(T)/cc-pVTZ (aug-cc-pVTZ for Cu, He) level of theory. For Cu(I)/UiO-66·He an effecttive core potential (ECP) was used for Zr atom. QTAIM properties calculated at the PBE0-D3(BJ)/TZ2P level; Hirshfeld Charges of the cluster models are given with adsorbed He* q_{CuHe} *(the charges of adsorbed He atom* q_{He} *are given in the square brackets). Electron Density* ρ_{BCP} *and its Laplacian* $\nabla^2{}_{BCP}$ *at the BCP between* Cu^+ *and He.*

Systems	d_{CuHe}(Å)		E^0_{ads} (kJ·mol^{-1})		$q_{CuHe}(e)$ [$q_{He}(e)$]	ρ_{BCP} ($e \cdot r_{\mathrm{Bohr}}$)	$\nabla^2{}_{BCP}$ ($e \cdot r_{\mathrm{Bohr}}$)
	^3He	^4He	^3He	^4He			
6c2	1.90	1.89	−9.2	−9.6	+0.481 [+0.110]	0.052	0.334
9c3	1.97	1.96	−5.9	−6.1	+0.395 [+0.093]	0.042	0.261
2*z*$^-$	2.23	2.21	−2.1	−2.3	+0.417 [+0.067]	0.023	0.130
3*z*$^-$	2.20	2.18	−3.4	−3.5	+0.458 [+0.072]	0.025	0.146
Cu(I)-MFU-4*l*	2.94	2.92	−0.8	−0.9	+0.267 [+0.019]	0.006	0.026
m20	3.75	3.74	−0.2	−0.3	+0.262 [+0.023]	0.002	0.010

Cu(I)Porphyrin	3.17	3.15	−1.8	−1.8	+0.583 [+0.023]	0.003	0.012
m2_CuCu	2.76	2.74	−1.5	−1.6	+0.451 [+0.034]	0.007	0.030
m2_CuZn	3.12	3.10	−0.7	−0.8	+0.327 [+0.022]	0.004	0.014
Cu(I)/UiO-66	2.35	2.33	−2.1	−2.3	+0.354 [+0.053]	0.014	0.071
m502_p3	2.11	2.09	−3.8	−4.1	+0.406 [+0.085]	0.032	0.186

MOFs offer an unprecedented diversity of structures, some of which can host Cu(I) sites. To assess these extended framework structures, suitable cluster models have been chosen for each MOF structure discussed below, which are described in detail in the Methods section. Among the MOFs, Cu(I)-MFU-4*l* has been studied intensively for its strong adsorption towards H_2[25,33] and its resulting separation capability of dihydrogen isotopologues.[24] Contrary to the strong interaction to H_2, there is only very weak attraction towards helium as indicated by a Cu-He distance of 2.72 Å, and a BO adsorption energy of −1.8 kJ·mol^{-1}. The resulting small ZPE differences of 0.13 kJ·mol^{-1} result in a separation factor of 1.3 at LH2 temperature**.** Another MOF well-investigated for its catalytical activity is Cu(I)/UiO-66[34] which can anchor isolated Cu(I) sites on defected Zr_6 nodes. These sites have been reported to be catalytically active for reactions such as CO oxidation[35]. This site binds helium more strongly compared to Cu(I)-MFU-4*l*, with a Cu–He distance of 2.33 Å and the corresponding BO adsorption energy of −3.4 kJ·mol^{-1}.The corresponding ZPE difference amounts to 0.17 kJ·mol^{-1}, which is comparable with that seen in zeolite 3*z*, resulting in a similar expected performance for ^{3}He/^{4}He separation.

To take advantage of the rich structural diversity of MOFs, we identified additional undercoordinated open Cu(I) sites by screening 952 inorganic secondary building units (SBUs) from the publicly available HEALED library,[36] which comprises a comprehensive set of experimentally synthesized MOF building blocks. Our initial filter targeted SBUs containing Cu

in the +1 oxidation state, yielding 31 candidates. Each candidate was then subjected to a coordination geometry analysis to determine which Cu(I) centers constitute plausible open metal sites. Sites with two or three coordinating ligands are classified as open by default. For four-coordinate complexes, we only considered them as open if their geometries adopt a seesaw or square planar arrangement. After an inspection of the structures identified, we select five SBUs – two bicoordinate, one tricoordinate and two tetracoordinate Cu(I) sites. We refer to these SBUs according to their identifiers in the HEALED library. Additionally, we consider two Cu(I) containing SBUs from the defected paddlewheel nodes of the Cu-BTC MOF(ref), as they have been found to be highly active towards CO adsorption.[37] All these SBUs except one show weak to no attraction towards helium as indicated by the Cu–He bond distance. Interestingly, m502_p3 (correspond CCDC entry WOLRIZ) shows an especially strong attraction for He as indicated by a Cu-He distance of 2.0 Å and BO adsorption energy of −5.9 kJ·mol^{-1} which is highest among all the zeolites and MOFs considered. The active site in m502_p3 is a bicoordinated Cu(I) bound to two tetrazolate ligands. The high activity of m502_p3 is attributed to the bent geometry around the active site with a N-Cu-N angle of 96.8° which facilitates He adsorption. By comparison, m20, which also features a very similar chemical environment - bicoordinated Cu(I) connected to pyrazolate ligands - adopts a linear geometry with N-Cu-N angle of 179.7° and as a result barely binds to He (BO adsorption energy −0.8 kJ/mol). The ZPE difference between the two helium isotopes in m502_p3 is 0.24 kJ·mol^{-1} yielding separation factors of 3.9 (1.3) at LH2 (LN2) temperature (Tab. S10).

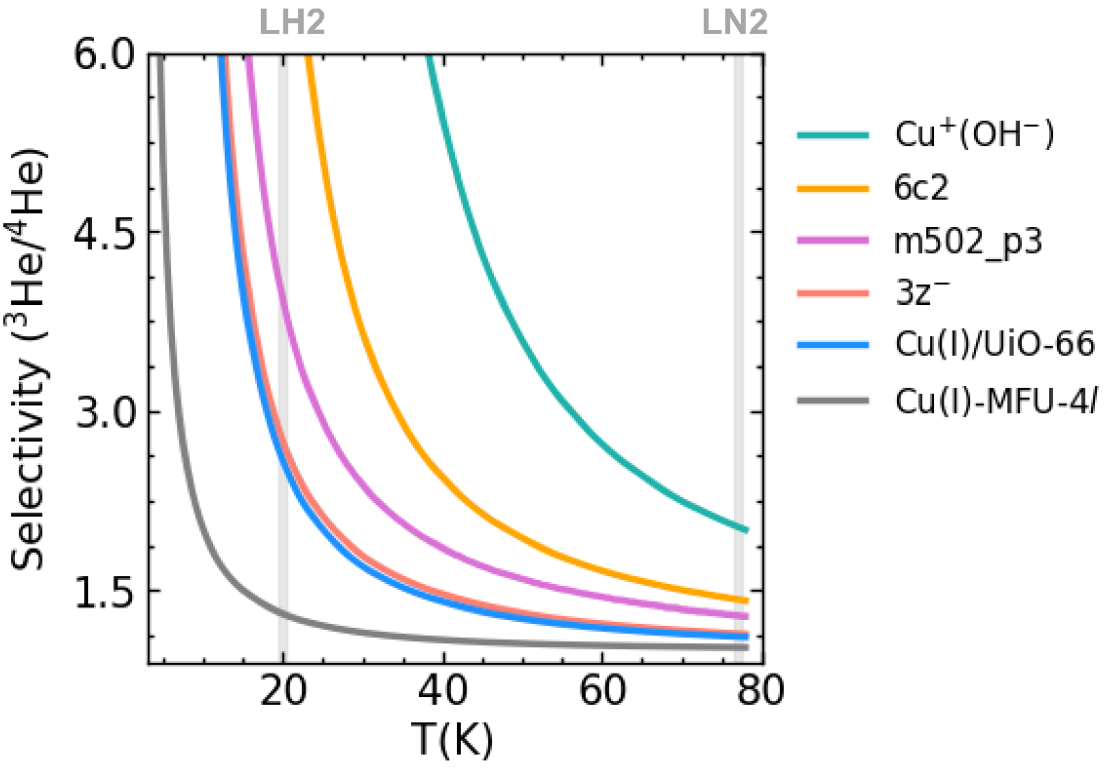


***Fig. 3**: Predicted separation factors for adsorptive He isotope on selected top-performing Cu(I)-candidates, plotted as a function of temperature.*

Summary

We have shown that helium, which is usually considered to be chemically inert, can have sizable interactions with Cu(I) sites. These polarization-based interactions are enforced by charge transfer from He to Cu. To illustrate the strength of interaction, the electron density given by a QTAIM analysis yields a value greater than twice the hydrogen bond in the water dimer and over twenty times that in the argon dimer. Complexes with Cu–He bond lengths of ~2 Å or less can show appreciable Born-Oppenheimer adsorption energies, reaching −5.9 kJ mol^{-1} for the best materials model, MOFs based on the SBU found in WOLRIZ. However, this value is less than half compared to that for small gas-phase complexes including Cu(I) (with a record-high value of −17.1 kJ mol^{-1}), suggesting that a further search may yield MOFs with active, undercoordinated metal sites that are even more promising for adsorptive He isotope separation.

The strong interaction energy gives rise to large nuclear quantum effects, sufficient to separate helium isotopes at the technically meaningful temperature of 20 K, the boiling temperature of H_2. The separation factor of 3.9 estimated for the best-performing MOF significantly exceeds the state of the art, which requires temperatures below 4 K and shows separation factors of 2 or less. We note that at the relevant temperatures for helium isotope separation, typical obstacles of highly reactive MOFs, namely the adsorption of residual water or other molecules or mechanical stability, are irrelevant. The same is true for the materials costs, as ^{3}He is one of the most expensive isotopes with increasing demand meeting a reduction of traditional production via the decay of tritium obtained from radioactive waste.

We note that while this work concentrates on Cu(I), it is likely possible that other active metal centers will attract helium with similar or even superior strength. We hope that this work will start a research endeavour with the aim to do chemistry with the most chemically innocent element on the planet, helium.

Methods

Gas phase model clusters

All Cu(I) complexes were fully optimized at the coupled-cluster singles, doubles, and perturbative triples excitations, CCSD(T), level of theory in conjunction with the augmented correlation-consistent polarized valence triple-ζ (aug-cc-pVTZ) basis set. Harmonic vibrational frequency calculations were then carried out for the fully optimized structures with and without adsorbed helium. ZPE were calculated (reported solely in Tab S3b) from the harmonic analysis. For energy calculations, including single-point calculations to establish the Cu-He bond potential, we corrected for basis set superposition errors in between He and the Cu(I)-hosting fragment. Calculations were performed with the Gaussian 16 program package.[38]

The analysis of the electron density was carried out using QTAIM approach. Calculations using the hybrid PBE0-D3(BJ) level with the Slater-type TZ2P basis set were performed with the Amsterdam Density Functional (ADF 2025) program.[39,40]

DLPNO-CCSD(T) single-point calculations were carried out in ORCA 5.0.1[41], using both TightSCF/TightPNO threshold settings (*i.e*, TightPNO settings with T_{cutMKN}, T_{cutPNO} and $T_{cutPairs}$

tightened to 10^{-6}, 10^{-8}, 10^{-7} respectively[42]. For the detailed explanation of these cutoff parameters, see ref.[43,44]). While we describe Cu and He with the aug-cc-pVTZ basis as in the canonical CCSD(T) calculations, we renounce the augmentation and use the cc-PVTZ basis for the other atoms for computational efficiency.

The protocol to calculate the numerical frequencies has been validated at the MP2/def2-TZVPP level of theory. This approach allows for the full geometry optimization followed by second-order vibrational perturbation theory (VPT2) calculation of the frequencies (Tab. 4). Note that while the MP2 calculations are not sufficient to accurately predict the interaction energies and partially the bond lengths, they are sufficient to analyze the vibrational modes and their couplings and thus to validate our numerical approach for the frequencies. The MP2 calculations have been performed using Gaussian 16[38].

For the numerical calculations, we first fitted the PES of the Cu-He bond to the one-dimensional Morse potential with a charge-induced dipole (CID) term, which is switched off for short distances via a Fermi function (for parameters and shape, see Fig. S1, Supplementary Note 1). The finite difference method (FDM)[45] was then applied to solve the one-dimensional Schrödinger equation (see details in the Supplementary Note 2). The results are on average by 16 cm^{-1} larger as those of the VPT2 calculations, which can be expected as the FDM calculations cover a longer range, while, on the other hand, neglect couplings to the other modes.

Tab. 4*: Harmonic and anharmonic VPT2 frequencies (cm^{-1}) of ^{4}He in small Cu(I)-complexes computed at* MP2/def2-TZVPP *level of theory. Numerical frequencies are also given.*

	Frequencies at MP2/def2-TZVPP level						
Systems	Modes	ν_{harm}^{full}	ν_{harm}^{He} 3DOFs[a]	$\nu_{numerical}^{MCID}$	ν_{VPT2}^{full}	ν_{VPT2}^{He} 3DOFs[a]	$\nu_{numerical}^{MCID}$
Cu^+He	ν_s	187.4	187.4	187.0	134.1	134.1	140.1
$Cu^+(OH^-)He$	ν_s	512.4	509.1	509.7	415.5	413.1	444.2
	$\nu_{\perp 1}$	226.9	191.2	191.0	231.5	177.6	190.5
	$\nu_{\perp 2}$	230.5	191.4	191.8	235.2	178.4	191.4

$Cu^+(H_2O)He$	ν_s	337.9	359.4	360.8	272.3	277.2	301.2
	$\nu_{\perp 1}$	118.7	101.0	101.1	109.0	89.5	100.9
	$\nu_{\perp 2}$	122.4	103.8	103.7	138.3	92.5	103.5
$Cu^+(H_2O)(OH^-)He$	ν_s	456.8	459.8	460.2	345.2	355.7	384.2
	$\nu_{\perp 1}$	162.8	162.7	162.4	148.2	152.4	161.7
	$\nu_{\perp 2}$	198.3	166.7	166.2	177.7	149.4	165.6

ν^{full}: frequencies obtained with full normal modes whereas ν^{He} keeps only the three motion adsorbed He
$\nu^{MCID}_{numerical}$: frequencies obtained using the FDM approach
3DOFs only the three degrees of freedom of adsorbed He atom are considered
$\nu_{\perp 1}$ and $\nu_{\perp 2}$ correspond to the orthogonal contribution modes of He atom; while ν_s represents the stretching vibrational mode.

Material models

The crown ethers, Cu(I)porphyrin zeolite and Cu(I)-MFU-4l[25] clusters were all taken from the literature[31,46]. He atom was initially positioned above the Cu(I) site at a reasonable distance, and subsequently optimized at the PBE0-D3/def2-TZVPP level of theory while freezing the rest of the atoms to refine the Cu-He bond distance. All calculations were performed using the Gaussian 16 program package.[38]

The structural model for the Cu(I)/UiO-66 (Fig. 2g) was curated from reference[35], which is based on the crystal structure of UiO-66.[34] As found in previous experimental reports, the Cu^+ ion is supported on a defective Zr_6 node of UiO-66 with a missing linker with the chemical formula of the node being $Cu(I)/Zr_6O_4(OH)_3(linker)_{11}(OH)_1$ where one Cu^+ ion and one hydroxyl group are placed to cap the defect site and a μ_3 hydroxyl proton is removed to maintain the charge neutrality of the cluster. Here, the benzenedicarboxylate linkers were replaced by formates to reduce computational costs. The active site for He binding features a two-fold coordinated Cu(I), bound to an oxygen atom from the OH ligands capping the defect site and a nearby μ_3 oxygen. The structural model is optimized at the PBE0-D3/def2SVP level of theory with the carbon atoms of the formate linkers fixed in order to mimic the constraints in the MOF environment.

The SBUs extracted from the HEALED library were capped with a protons at the node connection points. The proton positions were relaxed at PBE0-D3/def2SVP level of theory with the remainder of the cluster atoms fixed to their crystal positions. Two SBUs featuring bicoordinated Cu(I) sites, were refer as m20 and m502_p3, following their identifiers in the HEALED library. m20 (Fig. 2k), found in several copper pyrazolate-based MOFs, features a two-fold coordinated Cu(I) connected to pyrazolate ligands in a linear arrangement.[47] While the active Cu(I)-site in m502_p3 (Fig. 2h) found in WOLRIZ, adopts a bent geometry resulting from the coordination of two tetrazolate ligands.[48] On the other hand, for the defected paddlewheel SBUs, the corresponding SBU with the formula Cu2O8C4X4 (m2 and X being the node connection points) was extracted from the HEALED and capped with protons. One formate linker was removed to create the defected m2_CuCu (Fig. 2i) SBU. Furthermore, the one Cu^{2+} is replaced by Zn^{2+} to create the mixed metal m2_CuZn (Fig. 2j) SBU.

After all MOFs had been selected, a He atom was placed above the Cu(I) center so that the Cu–He bond was aligned along the framework's vertical axis and then, geometry optimizations were carried out at the PBE0-D3/def2-TZVPP level. Throughout the optimization, only the helium atom was relaxed, all other atoms remained frozen (see Fig 2).

Nuclear quantum effects and isotope separation factors

We only consider three degrees of freedom (DOF) for the NQE calculations, namely those related to the helium motion. For the Cu-He stretch vibration, anharmonicity is fully accounted for as the Schrödinger equation of the Cu-He stretch vibration was solved numerically using the FDM, using the reduced mass of the Cu-He moiety. The increase of Cu-He bond length is an additional result of the FDM calculation. The out-of-plane modes were treated using the harmonic approximation, calculated via a three-point potential fit.

The ^{3}He/^{4}He separation factors $\alpha(^3\text{He}/^4\text{He})$ are calculated via the equilibrium adsorption constants $K_{ad}(^3\text{He})$ and $K_{ad}(^4\text{He})$. These adsorption constants are obtained from the partition functions which have been calculated by multiplying the individual contributions from each of the three normal

modes based on the Langmuir model and the ideal gas approximation for translational partition function of free He (see details in the Supplementary Note 3).

$\alpha(^3He/^4He) = \frac{K_{ad}(^3He)}{K_{ad}(^4He)}$ where. $K_{ad}(^4\mathrm{He}) = \frac{q^{ad}_{^4\mathrm{He}}}{q^{g}_{^4\mathrm{He}}}$ and $K_{ad}(^4He) = \frac{q^{ad}_{^3He}}{q^{g}_{^3He}}$

Author contributions

Conceptualization T.H.; Methodology E.G.D., T.W., S.D., and T.H..; Investigation E.G.D; Data Curation E.G.D and S.D.; Analysis E.G.D, T. W., S.D and T.H.; Writing- Original Draft, E.G.D., T.W., S.D. and T.H..; Writing-Review and Editing, E.G.D., T.W., S.D. and T.H.; Supervision, Project Administration and Funding Acquisition, T.H.

Author Information

The authors declare no conflicts of interest.

Acknowledgements

This work was funded by the Deutsche Forschungsgemeinschaft (DFG), Project ID 443871192 – GRK 2721: "Hydrogen Isotopes, ^{1,2,3}H". EGD thanks the Center for Information Services and High Performance Computing (ZIH) at TU Dresden for computational resources.S.D. acknowledges funding from the Horizon Europe's Marie Skłodowska-Curie Actions (grant agreement ID. 101207236).

Data availability statement

The datasets generated in this work are available in the zenodo repository, under the accession code DOI: https://zenodo.org/records/16281167 . All other relevant data supporting the findings of this study are available from the corresponding author upon reasonable request.

References

1. Rzepa, H. S. The rational design of helium bonds. *Nature Chem* **2,** 390–393; 10.1038/nchem.596 (2010).
2. S. T. Soper. *Atomic polarizabilities* (Journal of Physics B: Atomic, Molecular and Optical Physics, 2002).
3. characterization of porous solids - lowell.
4. Huang, H., Ge, X., Yu, X., Jiang, Y. & Peng, Q. Atomistic studies of helium trapping and diffusion at Ni–graphene interfaces. *Eur. Phys. J. Plus* **140**; 10.1140/epjp/s13360-025-06447-1 (2025).
5. Chen, H. *et al.* Steady-State simulation of cryogenic distillation used for helium isotope separation. *Cryogenics* **139,** 103805; 10.1016/j.cryogenics.2024.103805 (2024).
6. Atmospheric helium isotope ratio.
7. Bulubașa, G. *et al.* Studies on helium-3 separation at Cernavoda nuclear power plant. *Fusion Engineering and Design* **146,** 398–401; 10.1016/j.fusengdes.2018.12.076 (2019).
8. Dai, Z. *et al.* Helium separation using membrane technology: Recent advances and perspectives. *Separation and Purification Technology* **274,** 119044; 10.1016/j.seppur.2021.119044 (2021).
9. helium_485573a.
10. helium_statistic_id729995_global-helium-consumption-distribution-by-end-use-2021.
11. Mazzucato, E. A D-3He fusion reactor for the mitigation of global warming. *Fundamental Plasma Physics* **6,** 100022; 10.1016/j.fpp.2023.100022 (2023).
12. Dai, Z. *et al.* Helium separation using membrane technology: Recent advances and perspectives. *Separation and Purification Technology* **274,** 119044; 10.1016/j.seppur.2021.119044 (2021).

13. Halperin, W. P. The impact of helium shortages on basic research. *Nature Phys* **10,** 467–470; 10.1038/nphys3018 (2014).

14. Wojciech Kempiński *et al.* Helium3 isotope separation and lambda front observation. *Separation and Purification Technology* **210,** 276–280; 10.1016/j.seppur.2018.08.003 (2019).

15. Kempiński, W. *et al.* When superfluidity meets superconductivity in the extraction of 3He isotope from liquid helium. *Scientific reports* **15,** 22822; 10.1038/s41598-025-05542-8 (2025).

16. Savchenko, I. *et al.* Hydrogen isotope separation in metal-organic frameworks: Kinetic or chemical affinity quantum-sieving? *Microporous and Mesoporous Materials* **216,** 133–137; 10.1016/j.micromeso.2015.03.017 (2015).

17. Oh, H. & Hirscher, M. Quantum Sieving for Separation of Hydrogen Isotopes Using MOFs. *Eur J Inorg Chem* **2016,** 4278–4289; 10.1002/ejic.201600253 (2016).

18. Sengupta, D. *et al.* Air-Stable Cu(I) Metal-Organic Framework for Hydrogen Storage. *Journal of the American Chemical Society* **145,** 20492–20502; 10.1021/jacs.3c06393 (2023).

19. Teufel, J. *et al.* MFU-4 -- a metal-organic framework for highly effective H(2)/D(2) separation. *Advanced materials (Deerfield Beach, Fla.)* **25,** 635–639; 10.1002/adma.201203383 (2013).

20. FitzGerald, S. A., Mukasa, D., Rigdon, K. H., Zhang, N. & Barnett, B. R. Hydrogen Isotope Separation within the Metal–Organic Framework Cu(I)-MFU-4 l. *J. Phys. Chem. C* **123,** 30427–30433; 10.1021/acs.jpcc.9b09332 (2019).

21. Kim, J. Y., Oh, H. & Moon, H. R. Hydrogen Isotope Separation in Confined Nanospaces: Carbons, Zeolites, Metal-Organic Frameworks, and Covalent Organic Frameworks. *Advanced materials (Deerfield Beach, Fla.)* **31,** e1805293; 10.1002/adma.201805293 (2019).

22. Ipek, B., Pollock, R. A., Brown, C. M., Uner, D. & Lobo, R. F. H 2 Adsorption on Cu(I)–SSZ-13. *J. Phys. Chem. C* **122,** 540–548; 10.1021/acs.jpcc.7b09963 (2018).

23. Xiong, R. *et al.* Highly effective hydrogen isotope separation through dihydrogen bond on Cu(I)-exchanged zeolites well above liquid nitrogen temperature. *Chemical Engineering Journal* **391,** 123485; 10.1016/j.cej.2019.123485 (2020).

24. Weinrauch, I. *et al.* Capture of heavy hydrogen isotopes in a metal-organic framework with active Cu(I) sites. *Nature communications* **8,** 14496; 10.1038/ncomms14496 (2017).

25. Yabuuchi, Y. *et al.* Geometric Tuning of Coordinatively Unsaturated Copper(I) Sites in Metal-Organic Frameworks for Ambient-Temperature Hydrogen Storage. *Journal of the American Chemical Society* **146,** 22759–22776; 10.1021/jacs.4c08039 (2024).

26. Dongmo, E. G. *et al.* Direct evidence for ligand-enhanced activity of Cu(i) sites. *Chem. Sci.* **15,** 14635–14643; 10.1039/D4SC04582C (2024).

27. Jin, J., Wulf, T., Jorewitz, M., Heine, T. & Asmis, K. R. Vibrational spectroscopy of Cu+(H2)4: about anharmonicity and fluxionality. *Physical chemistry chemical physics : PCCP* **25,** 5262–5270; 10.1039/D2CP05802B (2023).

28. Evans, C. J., Wright, T. G. & Gardner, A. M. Geometries and bond energies of the He-MX, Ne-MX, and Ar-MX (M = Cu, Ag, Au; X = F, Cl) complexes. *The journal of physical chemistry. A* **114,** 4446–4454; 10.1021/jp912027y (2010).

29. Sandler, I., Chen, J., Taylor, M., Sharma, S. & Ho, J. Accuracy of DLPNO-CCSD(T): Effect of Basis Set and System Size. *The Journal of Physical Chemistry A* **125,** 1553–1563; 10.1021/acs.jpca.0c11270 (2021).

30. Liakos, D. G., Guo, Y. & Neese, F. Comprehensive Benchmark Results for the Domain Based Local Pair Natural Orbital Coupled Cluster Method (DLPNO-CCSD(T)) for Closed- and Open-Shell Systems. *The journal of physical chemistry. A* **124,** 90–100; 10.1021/acs.jpca.9b05734 (2020).

31. Wulf, T. & Heine, T. Small Crown-Ether Complexes as Molecular Models for Dihydrogen Adsorption in Undercoordinated Extraframework Cations in Zeolites. *J. Phys. Chem. C* **124,** 9409–9415; 10.1021/acs.jpcc.0c02815 (2020).

32. Tian, Y.-B. *et al.* Oriented Growth of In‐Oxo Chain Based Metal‐Porphyrin Framework Thin Film for High‐Sensitive Photodetector. *Advanced Science* **8**; 10.1002/advs.202100548 (2021).

33. Denysenko, D., Grzywa, M., Jelic, J., Reuter, K. & Volkmer, D. Scorpionate-type coordination in MFU-4l metal-organic frameworks: small-molecule binding and activation upon the thermally activated formation of open metal sites. *Angewandte Chemie International Edition* **53,** 5832–5836; 10.1002/anie.201310004 (2014).

34. Trickett, C. A. *et al.* Definitive molecular level characterization of defects in UiO-66 crystals. *Angewandte Chemie International Edition* **54,** 11162–11167; 10.1002/anie.201505461 (2015).

35. Abdel-Mageed, A. M. *et al.* Unveiling the CO Oxidation Mechanism over a Molecularly Defined Copper Single-Atom Catalyst Supported on a Metal-Organic Framework. *Angewandte Chemie International Edition* **62,** e202301920; 10.1002/anie.202301920 (2023).

36. Gibaldi, M., Kwon, O., White, A., Burner, J. & Woo, T. K. The HEALED SBU Library of Chemically Realistic Building Blocks for Construction of Hypothetical Metal–Organic Frameworks. *ACS Appl. Mater. Interfaces* **14,** 43372–43386; 10.1021/acsami.2c13100 (2022).

37. St Petkov, P. *et al.* Defects in MOFs: a thorough characterization. *Chemphyschem : a European journal of chemical physics and physical chemistry* **13,** 2025–2029; 10.1002/cphc.201200222 (2012).

38. *Gaussian 16 (Revision C.01)* (Wallingford CT, 2016., 2016).

39. AMS 2023.1 SCM. *Theoretical Chemistry, Vrije Universiteit, Amsterdam, The Netherlands. http://www.scm.com. The Netherlands. http://www.scm.com ,*

40. Baerends, E. J. *et al.* The Amsterdam Modeling Suite. *The Journal of chemical physics* **162**; 10.1063/5.0258496 (2025).

41. Neese, F. The ORCA program system. *WIREs Comput Mol Sci* **2,** 73–78; 10.1002/wcms.81 (2012).

42. orca_manual_5_0_4.

43. Santra, G., Semidalas, E., Mehta, N., Karton, A. & Martin, J. M. L. S66x8 noncovalent interactions revisited: new benchmark and performance of composite localized coupled-cluster methods. *Physical chemistry chemical physics : PCCP* **24,** 25555–25570; 10.1039/d2cp03938a (2022).

44. Liakos, D. G., Sparta, M., Kesharwani, M. K., Martin, J. M. L. & Neese, F. Exploring the Accuracy Limits of Local Pair Natural Orbital Coupled-Cluster Theory. *Journal of chemical theory and computation* **11,** 1525–1539; 10.1021/ct501129s (2015).

45. Mazumder, S. *Numerical methods for partial differential equations. Finite difference and finite volume methods* (Academic Press, Amsterdam, 2016).

46. Chakraborty, R. *et al.* Quantum chemical modeling of hydrogen binding in metal-organic frameworks: validation, insight, predictions and challenges. *Physical chemistry chemical physics : PCCP* **26,** 6490–6511; 10.1039/d3cp05540j (2024).

47. Tu, B. *et al.* Reversible Redox Activity in Multicomponent Metal–Organic Frameworks Constructed from Trinuclear Copper Pyrazolate Building Blocks. *J. Am. Chem. Soc.* **139,** 7998–8007; 10.1021/jacs.7b03578 (2017).

48. Dincă, M., Dailly, A. & Long, J. R. Structure and Charge Control in Metal–Organic Frameworks Based on the Tetrahedral Ligand Tetrakis(4‐tetrazolylphenyl)methane. *Chemistry A European J* **14,** 10280–10285; 10.1002/chem.200801336 (2008).

Supplementary Files

This is a list of supplementary files associated with this preprint. Click to download.

- SICuHe20250724.pdf